

A CT SCANNER USING
COINCIDENCE TECHNIQUES

By

Victoria E. Finch

A thesis submitted in partial fulfillment of the
requirements for the degree of

Bachelor of Arts

Houghton College

May 2014

Signature of Author.....

Department of Physics
May 19, 2014

.....

Dr. Mark Yuly
Professor of Physics
Research Supervisor

.....

Dr. Brandon Hoffman
Associate Professor of Physics

A CT SCANNER USING COINCIDENCE TECHNIQUES

By

Victoria E. Finch

Submitted to the Department of Physics
on May 19, 2014 in partial fulfillment of the
requirement for the degree of
Bachelor of Arts

Abstract

A CT scanner has been designed which uses gamma rays produced by positron annihilation. A low-activity ^{22}Na source produces the positrons, which, when they annihilate, create 0.511 MeV gamma rays travelling in opposite directions. These gamma rays can be used to image an object using NaI detectors that are collinear with the source. Requiring a coincidence between the detectors reduces background. LabVIEW software counted the number of gamma ray coincidences and translated and rotated a robotic table, allowing the attenuation to be measured along multiple beam paths through the object. Ultimately, the attenuation data can be used to reconstruct an image of the object being observed.

Thesis Supervisor: Dr. Mark Yuly
Title: Professor of Physics

TABLE OF CONTENTS

Chapter 1. Introduction	6
1.1 Overview of the CT scanner	6
1.1.1 Tomography.....	6
1.1.2 Transmission CT scanner	7
1.2 History of the CT scanner	9
1.2.1 Cormack's initial theories	9
1.2.2 Hounsfield's initial experiments	9
1.2.3 Variations of CT technology	10
1.2.5 Second-Fourth generations of CT	10
1.2.6 Use of CT with other technology	11
1.3 Project Description and Motivation	12
1.3.1 The Project	12
1.3.2 Motivation	12
Chapter 2. Theory	13
2.1 Source and attenuation of gamma radiation	13
2.1.1 ^{22}Na decay	13
2.1.2 Attenuation	14
2.2 Image Reconstruction	17
2.2.1 Simple Back-projection	17
2.2.2 Fourier Transform	20
2.2.3 Filtered Backprojection and Series Expansion	22
Chapter 3. Scanner Construction	23
3.1 Setup of NIM Electronics	23
3.1.1 Data acquisition circuit	23
3.1.2 Timing Resolution	24
3.1.3 Energy Resolution	27
3.2 Table	27
3.3 Setup of Detectors	28
3.3.1 Alignment	28
3.1.2 Angle Calculation	29

Chapter 4. Conclusion	32
4.1 Summary.....	32
4.2 Future Plans	32
Appendix A. LabVIEW Block Diagram.....	34
References	36

TABLE OF FIGURES

Figure 1.	An image taken by Roentgen in his initial experiments.	7
Figure 2.	Basic setup of a CT scanner.....	8
Figure 3.	Parallel and fan-shaped beam paths through an object.....	8
Figure 4.	Basic setup of a first-generation CT scanner	10
Figure 5.	Setups of four generations of CT scanners	11
Figure 6.	Decay scheme of ^{22}Na and positron annihilation.....	13
Figure 7.	Attenuation in a uniform material	14
Figure 8.	Attenuation in a material divided into three voxels	16
Figure 9.	Finding the attenuation coefficients of each voxel	18
Figure 10.	The attenuation of x-ray beams through an object projected onto a plane	19
Figure 11.	A poor quality image created by adding the attenuation.....	21
Figure 12.	The setup of the NIM electronics.....	24
Figure 13.	Calibration of MCA for measurment of timing resolution.....	25
Figure 14.	Time difference between the detection of "simultaneous" gamma rays.....	26
Figure 15.	^{22}Na gamma ray energy spectrum	26
Figure 16.	The robotic table used to translate and rotate the object.....	27
Figure 17.	Setup of the detectors	28
Figure 18.	Detectors and ^{22}Na source in line with each other.....	29
Figure 19.	Angular width of gamma rays though an object.....	29
Figure 20.	The addition of lead shielding decreases the angular width.....	30
Figure 21.	Relationship between angular width and distance to the detectors.....	31
Figure 22.	LabVIEW block diagram (counting and horizontal motion)	34
Figure 23.	LabVIEW block diagram (rotating the table)	35

Chapter 1

INTRODUCTION

1.1 Overview of the CT scanner

Computed tomography (CT) measures the attenuation of radiation as it travels through an object. By using the measured attenuation coefficients, an image showing the relative absorption specific to regions of the object can be reconstructed. These images are most commonly used today to aid in medical diagnosis.

1.1.1 Tomography

The term “tomography” is used to describe the process of constructing an image of an object by taking multiple projections, or “slices,” through the object. Traditional x-ray tomography, for example, creates a two-dimensional image that is sharp in the desired plane and blurred elsewhere [1]. Such images were first produced by Wilhelm Röntgen in 1895 when he first discovered the x-ray [2]. Röntgen used these x-rays to create images by placing a dense object between an x-ray source and a photoluminescent screen [2]. An example of one of these first images is shown in Figure 1. Dense materials like bone are dark on the screen while the surroundings are lighter. These images are useful for identifying bone fractures, but their ability to differentiate between soft tissues is limited [3].

Computed tomography, on the other hand, allows two or three-dimensional images to be taken by using a computer to reconstruct an image using multiple different projections. The classification of computed tomography falls into two main categories [3]:

- *Transmission Computed Tomography (CT)* uses the attenuation of an x-ray beam that passes through an object in order to reconstruct an image, and

- *Emission Computed Tomography (ECT)* detects radiation emitted from a source within the object being imaged, calculating its attenuation as it passes through that object.

Though both types of tomography are commonly used for medical imaging today, the term “computed tomography,” or “CT,” is mostly used to indicate transmission computed tomography. Common ECT imaging devices include positron emission tomography (PET) and single photon emission computed tomography (SPECT) scanners.

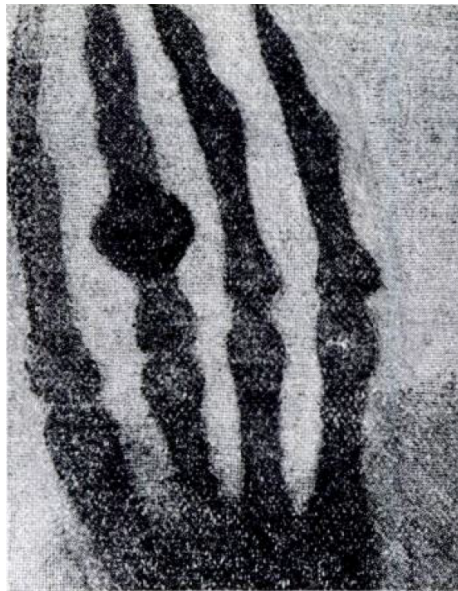


Figure 1. An image of a hand (with a ring on the third finger) taken by Roentgen in his initial experiments. Because the attenuation coefficient for bone is so large, the bone appears black on the film while softer tissues and air appear lighter. Figure taken from Ref. [2].

1.1.2 Transmission CT scanner

A simplistic design for a transmission CT scanner is shown in Figure 2. An x-ray source emits x-rays of known intensity, which then pass through an object. The intensity of the x-ray beam emerging from the object is measured by a scintillation detector. This process is described in more detail in Section 3.1.

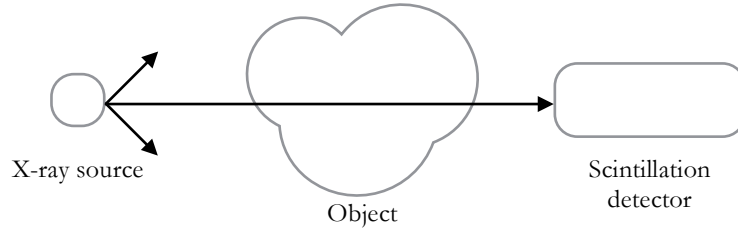


Figure 2. Basic setup of a CT scanner. The attenuation of the x-ray beam through the object is calculated after measuring the emerging intensity with a scintillation detector.

In order to reconstruct an image of the object, multiple projections are needed. This can be accomplished by moving the object (as done in a first-generation CT scanner) or by moving the source, collimators, and detector. The object, for example, might be translated so that data can be collected along multiple parallel or fan-shaped beams, shown in Figure 3. Then the object is rotated and a new set of projection data are obtained.

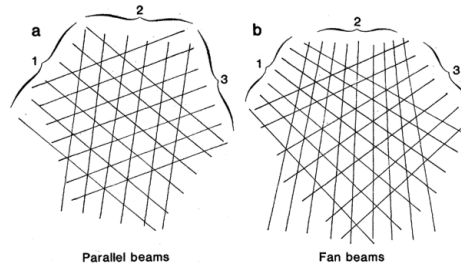


Figure 3. The beam paths taken can either be parallel, such as those in (a) or fan-shaped, such as those in (b). Parallel beam paths are obtained by translating the beam relative to the object multiple times, then rotating the reference frame and repeating the same procedure. Fan-shaped beam paths are seen by rotating the beam relative to the object. Figure taken from Ref. [4].

Measuring the incident and emerging beam intensity passing through the object along each of the beam paths illustrated in Figure 3, it is possible to find the attenuation coefficients along those beams. These data can then be used to reconstruct an image of the object using one of many back-projection methods. Examples of reconstruction processes are described further in Section 2.2.

1.2 History of the CT scanner

Before the invention of the transmission CT scanner in the 1970's, medical imaging techniques were limited [5]. Conventional x-ray tomography methods like Röntgen's allowed bones to be imaged on plane films, and angiography techniques looked at blood flow in order to detect tumors in the brain [5]. Though these developments made it possible to differentiate a bone from its surroundings, it was not until the development of higher-resolution CT and MR technologies that it became possible to differentiate between different "soft tissues" such as organs in the body [4].

1.2.1 Cormack's initial theories

In 1955 Allan Cormack began work on using the exponential attenuation of x- and gamma rays as they passed through a material for CT [6]. The familiar equation for the attenuation of x-rays travelling a distance x through a medium, $I = I_0 e^{-\mu x}$, can be solved for the attenuation coefficient μ . If a beam of intensity I_0 is incident on an object, and the emerging beam has a measured intensity of I , then the integral of the absorption coefficient μ along a line that passes through the object along a line L can be found by

$$\int_L \mu \, dl = -\ln \frac{I}{I_0}. \quad (1.1)$$

The Radon Transform, which was discovered in 1917 [7], can be used to solve this problem for $\mu(x, y)$ within the object. This is described in more detail in Chapter 2.

1.2.2 Hounsfield's initial experiments

Godfrey Hounsfield began to put Cormack's theories into practice. His first CT scanner used a low-intensity gamma source and detectors that rotated around an object to measure the incident and emerging intensity of the beam [4]. His device took 9 days to gather enough information about the object, and another 2 ½ days to reconstruct an image. Replacing the gamma source with an x-ray tube

allowed for a much shorter scanning time of 9 hours and better image quality. In 1972, the first hospital-quality CT scanner was tested, having a scanning time of just 18 seconds. By 1980, CT technology had already been implemented in more than a thousand hospitals worldwide [4].

1.2.3 Variations of CT technology

At his Nobel speech in 1979, Hounsfield spotlighted three different types of CT scanner that were in use [8]. The first generation of CT scanner, for example, uses a stationary source and detector in conjunction with a moving object that translates and rotates to obtain attenuation data from parallel or fan-shaped “slices” through an object. Using reconstruction methods described in Section 2.2, an image is formed from these slices. Figure 4 (which is similar to the design described in this paper) uses a rotating table to gather data from these x-ray beam “slices” through the object.

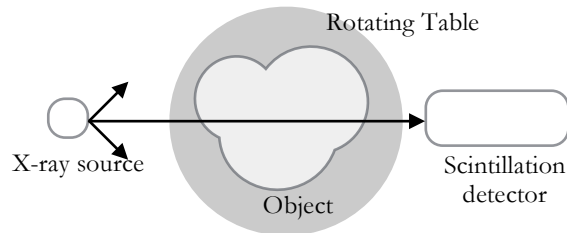


Figure 4. Basic setup of a first-generation CT scanner. A rotating table is used to gather attenuation data for multiple line paths through the object.

Later generations of CT scanners used detectors that rotate around one central location, or a source that rotates around an object while stationary detectors measure the emerging intensity of the beam.

1.2.5 Second-Fourth generations of CT

While the first generation of CT scanner is simple with its use of one detector and pencil-thin beams, it usually takes a long time to produce a low-resolution image. The second generation CT scanner, as shown in Figure 5, uses a fan-shaped beam and multiple detectors to provide higher-resolution images quickly.

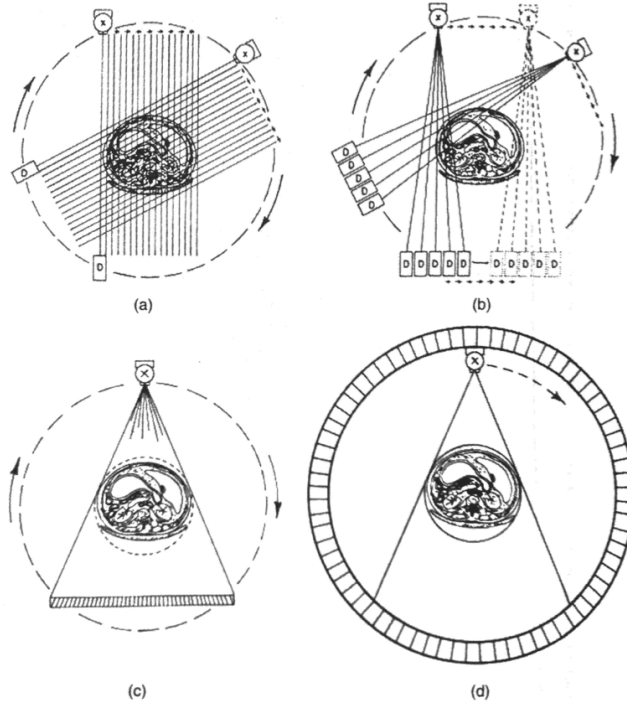


Figure 5. Setups of (a) first-generation (b) second-generation (c) third-generation and (d) fourth-generation CT scanners. Image taken from Ref. [9].

Third- and fourth-generation CT scanners eliminated the need to translate the detectors by rotating a large fan-shaped beam and using multiple detectors to look at the number of rays transmitted through the object. While third-generation scanners rotate the detectors with the source, fourth-generation scanners use more detectors aligned in a stationary ring while rotating the beam source around the ring [9].

1.2.6 Use of CT with other technology

While CT scanners still remain a cost-effective alternative to Magnetic Resonance (MR) techniques in diagnosis, they are also useful in combination with other medical technology, such as in combination with positron-emission tomography (PET) in order to provide a more precise localization of a tracer material in a patient's body [10]. Recent efforts have combined conventional CT scans with single photon-emission computed tomography (SPECT) in the same manner [10].

1.3 Project Description and Motivation

1.3.1 The Project

The CT scanner currently being built at Houghton College uses a low-intensity gamma ray source instead of the more traditional x-ray source used in CT scanners. By using a ^{22}Na source and two NaI detectors placed 180° apart, the gamma rays passing through an object can be measured in coincidence with another gamma ray emitted simultaneously by the source. A motorized table is placed between the detectors so the object can be translated and rotated in order to gain information about each parallel beam through the object. A LabVIEW Virtual Instrument (VI) was created to move the table and count the gamma ray coincidences.

1.3.2 Motivation

This project uses a low-intensity ^{22}Na source, unlike the traditional x-ray source used by CT scanners described in Section 1.1.2. The source produces relatively high-energy gamma radiation, 511 keV, as opposed to ~ 50 keV produced by a traditional x-ray tube. This allows for a smaller radiation dosage; since higher-energy rays are more likely to pass through the object, the object needs to be bombarded with fewer gamma rays to achieve the same count rate.

Because a low-intensity source is used, however, the effect of unwanted background radiation on the attenuation calculation would be large without the use of coincidence techniques. A second detector placed in line with the source and first detector counts the number of coincidence events to calculate the attenuation in the object. Since it is unlikely that background gamma rays would trigger both detectors simultaneously, this greatly reduces the background count rate.

Chapter 2

THEORY

2.1 Source and attenuation of gamma radiation

2.1.1 ^{22}Na decay

A ^{22}Na source was used because it emits two high-energy gamma rays back-to-back, allowing two detectors to be placed in line with the source.

The decay scheme for ^{22}Na is shown in Figure 6(a). Ninety percent of decays produce a positron. The positron then interacts with electrons in the surrounding environment and annihilates, producing two 0.511 MeV gamma rays. In order to conserve momentum, the emission of the two gamma rays, shown in Figure 6(b), must be at 180° in the center of momentum frame, which is the lab frame for positrons that have been slowed down.

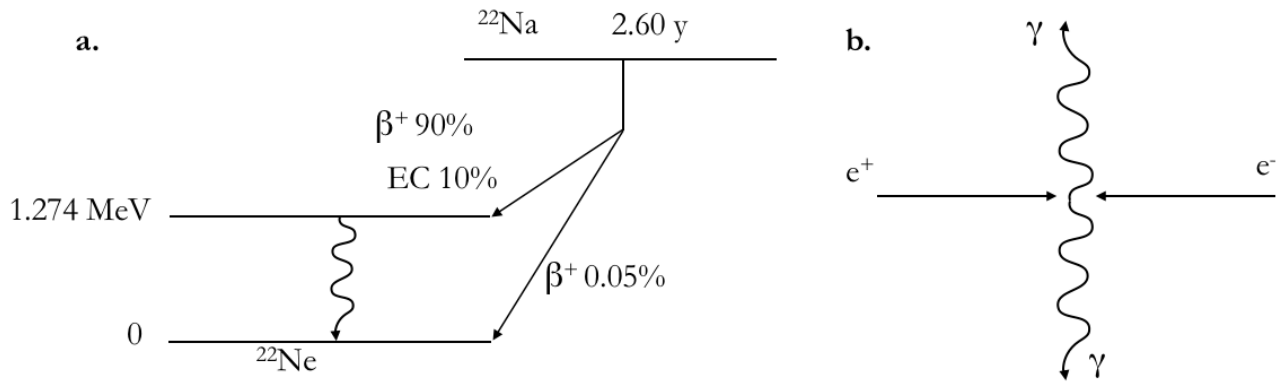


Figure 6. (a) Decay scheme of ^{22}Na [11]. (b) Annihilation of positron with electron, producing two antiparallel 0.511 MeV gamma rays in the center of momentum frame.

2.1.2 Attenuation

As a photon beam passes through a homogeneous material, it is attenuated so the emerging beam intensity I is given by

$$I = I_0 e^{-\mu x}, \quad (2.1)$$

where μ is the linear attenuation coefficient of the material and x is the distance the beam travels through the material. The value of μ determines how much the intensity of the beam will decrease travelling through a given distance x , assuming μx is constant along a line drawn through the object.

For the purposes of this paper, “attenuation” refers only to “linear attenuation”—which can also be found by multiplying the mass attenuation coefficient of a material by the density of that material.

Consider bombarding a material of thickness l with N_0 particles.

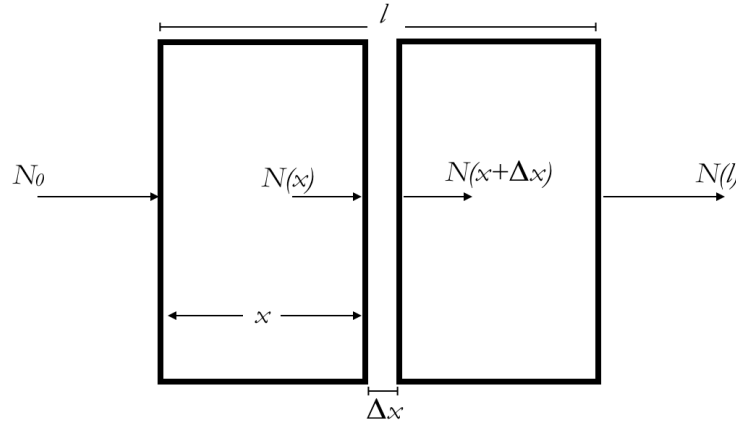


Figure 7. A material of thickness l is bombarded with N_0 particles. The attenuation in a thin slice Δx can be integrated to give the attenuation in distance l .

In Figure 7, $N(x)$ is the number of gamma rays present at a distance x into the material. We can isolate a region of interest Δx , and find the number of particles that stop in this region:

$N(x) - N(x + \Delta x)$. For a very thin slice Δx , the number that stop is proportional to both the thickness Δx and the number incident $N(x)$. The constant of proportionality we call μ , the attenuation coefficient.

$$N(x) - N(x + \Delta x) = \mu N(x) \Delta x. \quad (2.2)$$

Rearranging this equation and taking the limit as $\Delta x \rightarrow 0$ gives:

$$-\mu N(x) = \lim_{\Delta x \rightarrow 0} \frac{N(x + \Delta x) - N(x)}{\Delta x}, \quad (2.3)$$

$$-\mu N(x) = \frac{\partial}{\partial x} N(x), \quad (2.4)$$

which allows the number of gamma rays to be determined as a function of distance into the material,

$$N(x) = k e^{-\mu x}. \quad (2.5)$$

The boundary condition at $x = 0$ is that $N(x) = N_0$, the initial number of gamma rays, yielding

$$N(x) = N_0 e^{-\mu x}. \quad (2.6)$$

which is Equation 2.1.

The emerging beam intensity after passing through an object that does not have a constant attenuation coefficient is shown in Figure 8.

Applying Equation 2.1 to the first voxel of Figure 8 tells us

$$I_1 = I_0 e^{-\mu_1 x_1}. \quad (2.7)$$

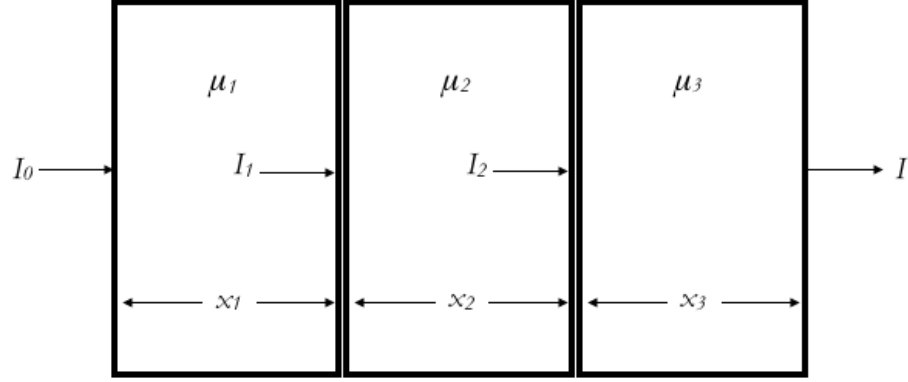


Figure 8. A material is bombarded with intensity I_0 . The material is divided into three voxels of widths x_1 , x_2 , and x_3 with coefficients μ_1 , μ_2 , and μ_3 , respectively.

Likewise,

$$I_2 = I_1 e^{-\mu_2 x_2}, \text{ and} \quad (2.8)$$

$$I = I_2 e^{-\mu_3 x_3}. \quad (2.9)$$

Clearly, Equation 2.9 can be re-written

$$I = I_0 e^{-\mu_1 x_1} e^{-\mu_2 x_2} e^{-\mu_3 x_3} = I_0 e^{-\sum_{i=1}^3 \mu_i x_i}. \quad (2.10)$$

For a material with n different attenuation coefficients,

$$I = I_0 e^{-\sum_{i=1}^n \mu_i x_i}, \quad (2.10)$$

where i sums over the product of the material's linear attenuation coefficient μ_i and the distance the beam travelled through the material x_i . If the distance x_i is very small, we can integrate the attenuation $\mu(x)$ along the line l :

$$I = I_0 e^{-\int_l \mu(x) dx} . \quad (2.11)$$

Using measured values for I and I_0 , this equation can be re-written to find the integral:

$$\int \mu(x) dx = \sum_{i=1}^n \mu_i x_i = -\ln \frac{I}{I_0} . \quad (2.12)$$

Using this relation, the value of μ may eventually be found for each location within the object. The value of μ as a function of position, $\mu(x,y)$, reconstructs an image of the object.

2.2 Image Reconstruction

In order to produce an image from the projections collected by a CT scanner, a back-projection method can be used. The most commonly used method of reconstructing images from the data collected by a CT scanner is filtered back-projection [12]. However, it is easier to understand the theory behind this technique by first discussing the method of simple back-projection.

2.2.1 Simple Back-projection

In this method, the incident and emerging beam intensities are measured in order to find the sum of all attenuation coefficients along that beam. After taking data along multiple beam paths through the object, the object is divided into equally spaced voxels as shown in Figure 9.

For a simplistic example like this, the attenuation of each voxel can be found in a way similar to solving a Sudoku puzzle [13] by using a trial-and-error approach to finding attenuation values. The attenuation values found for each voxel along a line must sum to equal the total attenuation measured along that line. The resultant matrix of each voxel's attenuation can be translated to an image that shows the variation in relative density of the material.

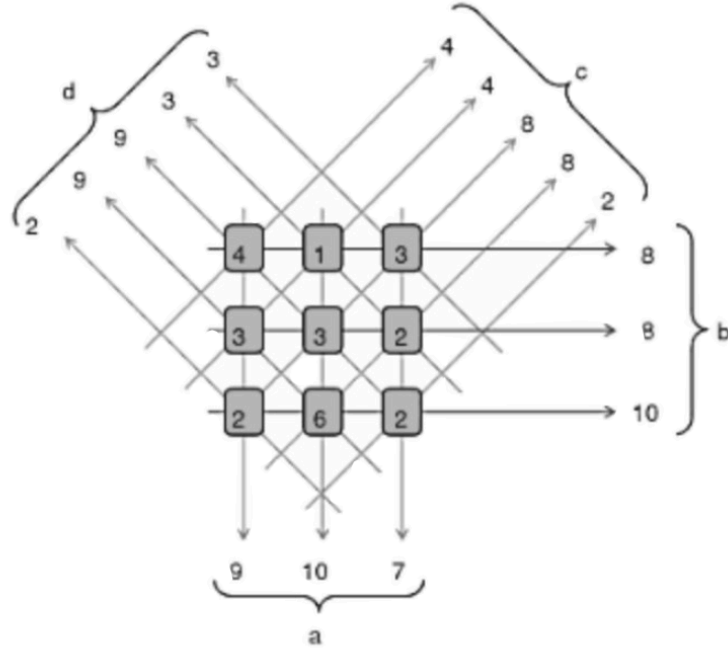


Figure 9. Illustrates the use of equally-spaced beams and corresponding projection data in order to find the attenuation coefficients of each voxel. Integer values were assigned to show the calculation of attenuation values using a trial-and-error approach so that the attenuations of each voxel along a line are summed to equal the total measured attenuation along that line. Figure taken from Ref. [14].

To find the value of μ for an object divided into more voxels the integral in Equation 2.12 is solved.

To do this, a projection function $P(t, \theta)$ is found as shown in Figure 10, where the coordinates in the (t, s) coordinate system are related to those in the (x, y) system by

$$t = x \cos \theta + y \sin \theta, \text{ and} \quad (2.13)$$

$$s = y \cos \theta - x \sin \theta. \quad (2.14)$$

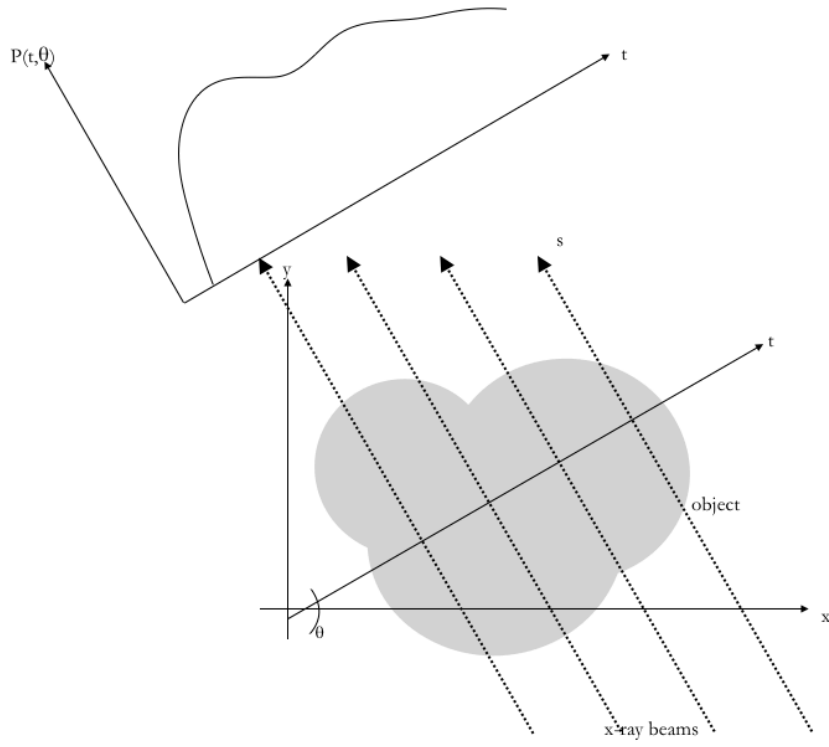


Figure 10. The attenuation of x-ray beams through an object $P(t, \theta)$ is found, where P describes the measured intensity of a ray at each (t, θ) .

If we define $P(t, \theta)$ to be

$$P(t, \theta) \equiv \int_L \mu(x, y) ds = -\ln \frac{I}{I_0}, \quad (2.15)$$

the Radon Transform can be written

$$P(t, \theta) = \int_{-\infty}^{\infty} \int_{-\infty}^{\infty} \mu(x, y) \delta(x \cos \theta + y \sin \theta - t) dx dy. \quad (2.16)$$

To make an image, $\mu(x, y)$ is obtained from the measured $P(t, \theta)$ using the inverse Radon transform

$$\mu_{BP}(x, y) = \int_0^\pi P(t, \theta) d\theta, \quad (2.17)$$

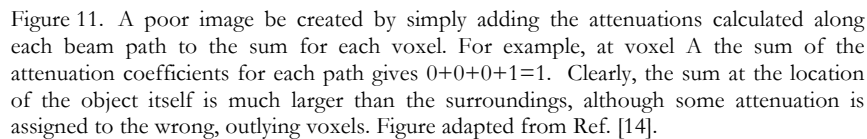
where $\mu_{BP}(x, y)$ is the backprojection of $\mu(x, y)$. Using equation 2.16, this becomes

$$\mu_{BP}(x, y) = \int_0^\pi \int_{-\infty}^\infty \int_{-\infty}^\infty \mu(x', y') \delta(x' \cos \theta + y' \sin \theta - t) dx' dy' d\theta, \text{ where} \quad (2.18)$$

$$t = x \cos \theta + y \sin \theta. \quad (2.13)$$

Computer programs that calculate the attenuation of each voxel from projection data would do so in a similar manner. Even by simply summing all attenuation projection data taken at each voxel, a very poor image can be created showing relative densities at specific regions within the object. This process is shown in Figure 11, where an object of attenuation $\mu=1$ is placed in the center of the scanned region and the surrounding attenuation is near $\mu=0$.

The image reconstructed using this technique assigns attenuation to the surrounding areas where $\mu=0$. A scaled image can be created from the measured attenuation values where the lowest data values in the matrix are represented as black and the highest values are represented as white. For an object with little variation in μ , the reconstructed image will be similar to an image created using the true attenuation values.



2.2.2 Fourier Transform

$$S(\omega, \theta) \equiv \int_{-\infty}^{\infty} P(t, \theta) e^{-2\pi i \omega t} dt, \quad (2.19)$$

21

$$S(\omega, \theta) = \int_{-\infty}^{\infty} \int_{-\infty}^{\infty} \mu(t, s) e^{-2\pi i \omega t} dt ds. \quad (2.20)$$

Using Equations 2.13 and 2.14, we can put Equation 2.20 in (x,y) coordinates:

$$S(\omega, \theta) = \int_{-\infty}^{\infty} \int_{-\infty}^{\infty} \mu(x, y) e^{-2\pi i \omega (x \cos \theta + y \sin \theta)} dx dy. \quad (2.21)$$

The inverse Fourier transform gives $\mu(x, y)$:

$$\mu(x, y) = \int_{-\infty}^{\infty} \int_{-\infty}^{\infty} S(\omega, \theta) e^{+2\pi i \omega (ux + vy)} du dv, \quad (2.22)$$

where $u = \omega \cos \theta$ and $v = \omega \sin \theta$.

Using this method, $P(t, \theta) = -\ln \frac{I}{I_0}$ is measured and Equation 2.19 is used to determine $S(\omega, \theta)$ by integrating over angle θ . The function $S(\omega, \theta)$ is used in Equation 2.22 to find the attenuation coefficient.

2.2.3 Filtered Backprojection and Series Expansion

Two alternative methods of reconstructing an image can be used. Filtered backprojection uses the same methods discussed in Section 2.2.1, correcting for the blur found in simple backprojection with the mathematical convolution function.

Series expansion uses algebraic techniques to divide attenuation data collected along a ray into equally spaced elements. Data taken at multiple angle orientations representing the same voxel are compared with each other and the difference in attenuation is added to each element [12].

Chapter 3

SCANNER CONSTRUCTION

3.1 Setup of NIM Electronics

Section 1.1.2 described a transmission CT scanner that measures the attenuation through an object using an x-ray source of known intensity and a scintillation detector. Whereas the CT scanner in Figure 4 used one scintillation detector and an x-ray source of large intensity, our setup uses a low intensity ($\sim 1 \mu\text{Ci}$) ^{22}Na source. To minimize the effect of background radiation, a second detector is used in coincidence; placed at a distance where if an annihilation gamma ray enters one detector its conjugate gamma ray will enter the other.

3.1.1 Data acquisition circuit

Two Bicron 2 inch diameter by one inch thick NaI detectors were placed in line with the source to detect the emitted gamma rays. Harshaw Preamplifier bases were attached to these detectors and the outputs were connected to ORTEC Model 455 Amplifiers, as shown in Figure 12.

Two ORTEC Model 455 Timing Single Channel Analyzers (TSCA's) were used to create logic pulses every time a 0.511 MeV gamma ray was detected. By using an oscilloscope to look at the amplifier pulses produced by a ^{22}Na source placed directly on the detector, the upper and lower limits of the TSCA were set so that pulses outside of the 0.511 MeV band shown did not generate a logic pulse.

Two National Instruments USB-6008 DAQ's controlled by the LabVIEW vi shown in Appendix A were used to count the number of coincidences with the same computer that controls the motion of the table. The program outputs an array containing the position of the detectors relative to the object and the number of coincidences seen at that position. One DAQ counted the output of SCA #3 (the

number of coincidences) while, as a monitor, a second counted the output of the SCA #1 (the number of pulses seen by detector 1).

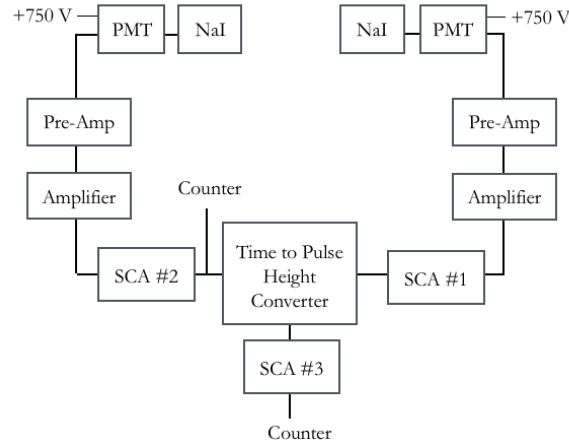


Figure 12. The setup of the NIM electronics. Two NaI detectors were used to detect ^{22}Na gamma rays. Corresponding logic signals were used to start and stop the TAC, which was connected to a SCA to generate a logic pulse for “simultaneous” events.

The ORTEC Model 437A Time to Pulse Height Converter (TAC) was used to generate a pulse whose height was proportional to the time difference between detectors 1 and 2. An ORTEC Model 413 Strobed Single Channel Analyzer (SCA) produced a logic pulse every time the time difference was less than a preset amount, thereby giving a logic pulse for “simultaneous” events.

3.1.2 Timing Resolution

The timing resolution of the electronics was measured using an AMPTEK Multichannel Analyzer (MCA-8000A). The MCA was calibrated by using the output of one of the detectors. The detector output started the TAC, but was also connected to a delay set to known time intervals which stopped the TAC.

Coincidence pulses from the TAC were seen from 0 to about 300 ns and used to calibrate the MCA, as seen in Figure 14.

From the timing peak in Figure 14, the FWHM was measured to be 41.3 ns.

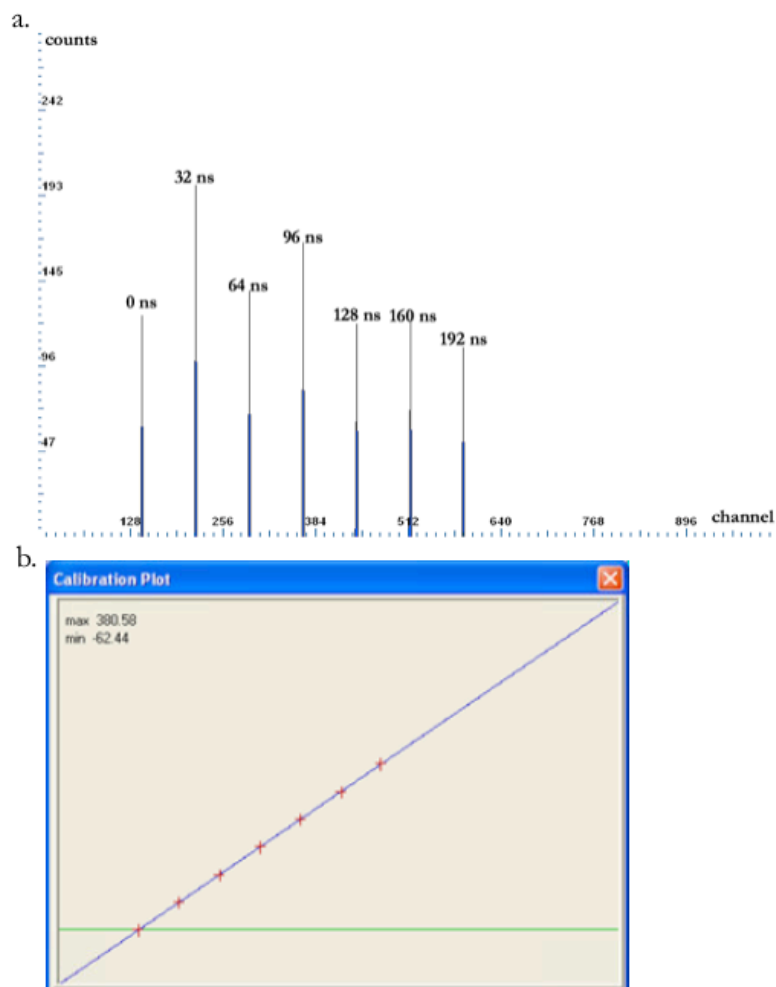


Figure 13. (a) Individual peaks are seen for each delay setting used to calibrate the MCA. (b) A linear calibration was applied using the channel values obtained for each delay time in Figure 13a.

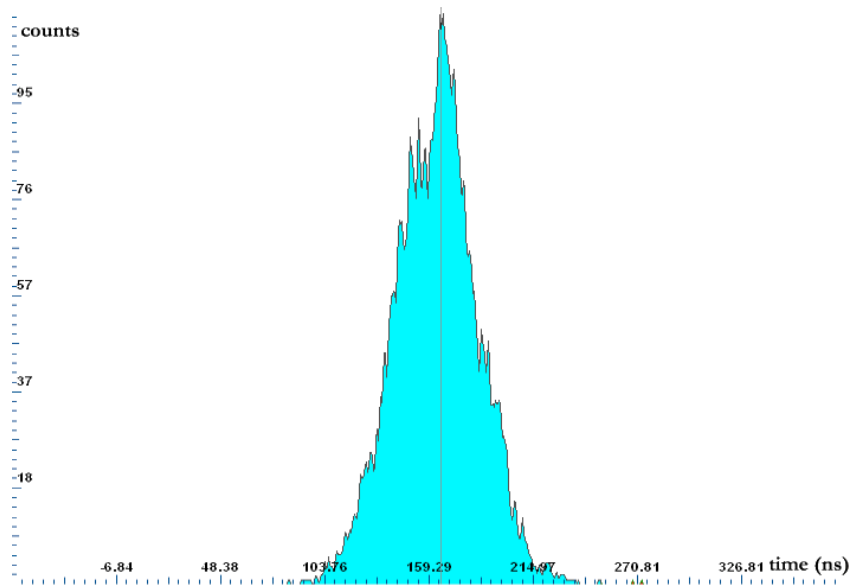


Figure 14. A peak is seen corresponding to the average time difference (around 160 ns) between the detection of “simultaneous” gamma rays in detectors 1 and 2. The FWHM is about 41.3 ns.

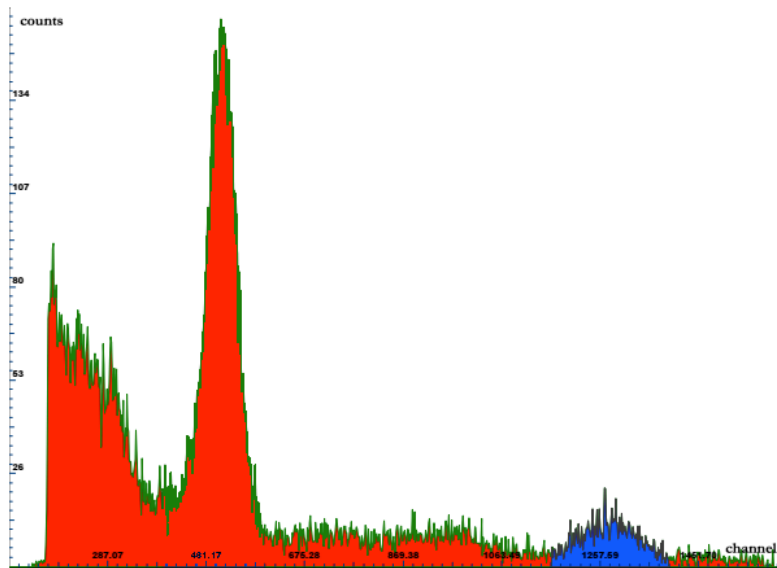


Figure 15. The shaded peak corresponds to 511 keV gamma rays. The energy resolution is 60.5 keV.

3.1.3 Energy Resolution

In order to see the detectors' energy resolution, the output of the amplifier was connected to the AMPTEK MCA and a ^{22}Na source was placed directly on the detector. The MCA was roughly calibrated linearly assuming the peak was due to 511 keV gamma rays and the MCA channel 0 was 0 MeV.

Looking at the 511 keV peak shown in Figure 15, a FWHM was measured of 60.5 keV, or about 12%.

3.2 Table

An Arrick Robotics RT-12 table was used to rotate the object with a stepper motor. This was bolted to the movable plate of an Arrick Robotics X-18 linear positioner, as shown in Figure 16.

Both motors were connected to an Arrick Robotics MD-2 dual stepper motor driver, which was connected via USB to a computer running LabVIEW to control the rotation and translation of the table. The block diagram for the LabVIEW program used is shown in Appendix A.

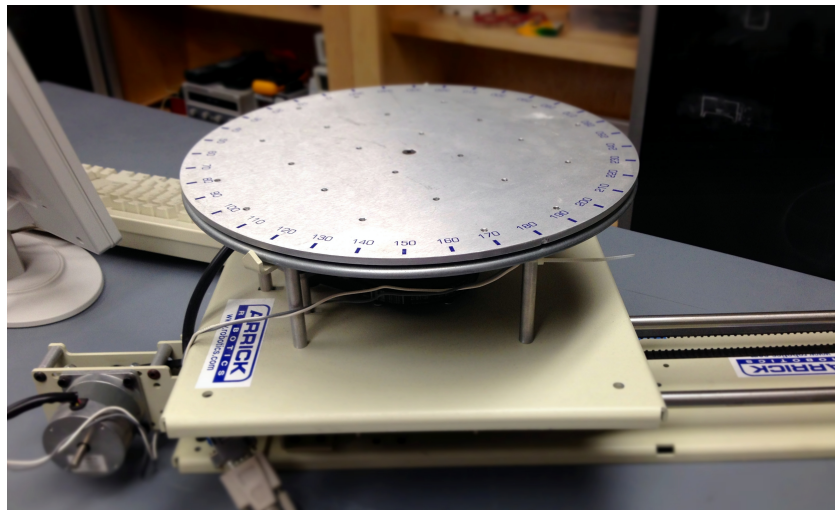


Figure 16. An Arrick Robotics RT-12 table was connected to an Arrick Robotics X-18 linear positioner to translate and rotate an object between the detectors.

3.3 Setup of Detectors

Since ^{22}Na releases gamma rays that are 180° apart, the detectors were aligned by making sure the two detectors were placed along a line with the source. In order to maximize the number of coincidences, it was also important to make sure the angular acceptances of the detectors were equal.

3.3.1 Alignment

The setup is shown in Figure 17, where detector 1 was used to measure the attenuation of the gamma rays through the object for gamma rays in coincidence with gamma rays detected by detector 2.

In order to measure gamma rays emitted from the source simultaneously, the detectors were placed 180° from the ^{22}Na source. The detectors were clamped to a 2.5 cm diameter aluminum rod (as shown in Figure 18) in order to keep them in line with each other.

A lead brick was placed in front of detector 1 with a 1 cm diameter hole drilled in it. The center of the detector was marked so it could be positioned in line with the hole drilled in the lead shielding. The shielding was aligned by shining a light source through the hole and making sure the mark was centered.

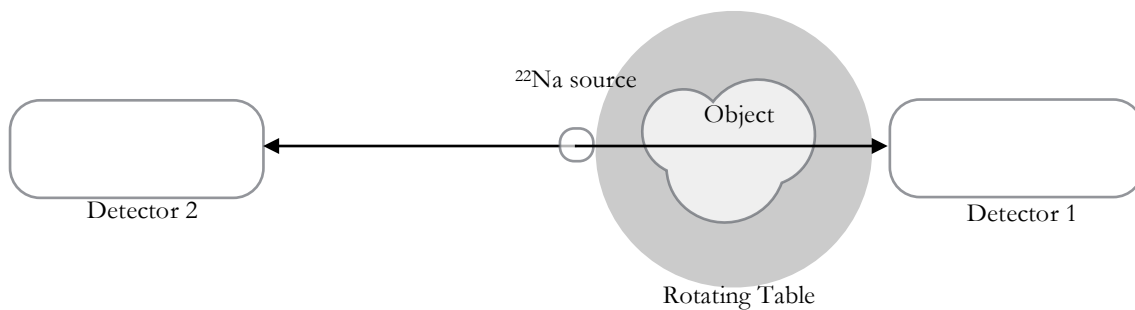


Figure 17. Setup of the detectors. Two Bicron NaI detectors were used, placed 180° apart.

Similarly, lead sheets with a 0.9 cm hole drilled in them were centered in front of detector 2. Two smaller rods (approximately 0.63 cm diameter) were clamped to either side of the detector to maintain the alignment of the shielding if detector 2 was repositioned.

A laser level was placed on the table below and the ^{22}Na source and detector 2 were moved to be in line with detector 1 and the source.

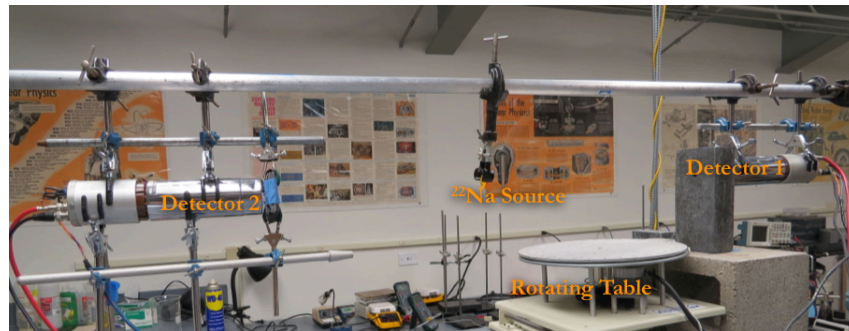


Figure 18. Detectors and ^{22}Na source in line with each other. Detectors were suspended from a large aluminum rod that was clamped to the table. Smaller rods were used to keep the detectors and lead shielding in line with each other.

3.1.2 Angle Calculation

If the detectors were placed too close to the ^{22}Na source, the gamma radiation passing through the object would not have the “pencil-thin” widths discussed in Section 2.2.2. Instead, a fan-shaped slice of the object would be seen, as shown in Figure 19.

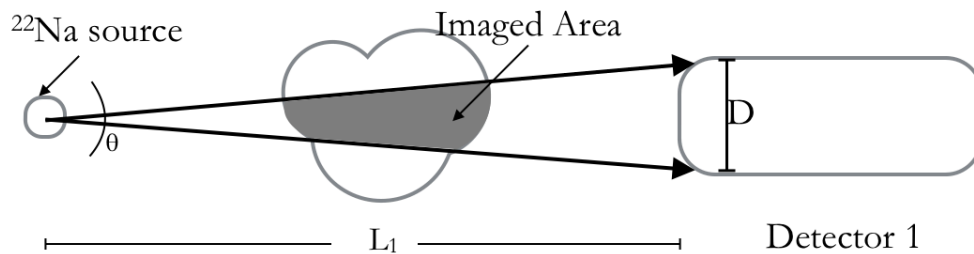


Figure 19. Two-dimensional cross section of the “slice” through the object. Here θ represents the angular width of this fan-shaped “slice.”

Since the detector and source were placed at either end of the rotating table of diameter 30.5 cm, the distance to detector 1 was $L_1=30.5$ cm. The diameter of each detector $D=5.5$ cm, giving an angle θ of 10.4° .

Two pieces of lead shielding were put in front of detectors 1 and 2 with holes drilled of diameters d_1 and d_2 , respectively, in order to reduce the angular acceptance. Their distances from the ^{22}Na source, L_1 and L_2 , are shown in Figure 21.

The lead brick with a hole drilled in it (diameter $d_1=1.036$ cm) was centered in front of detector 1 to give an angle of 0.97° . This is much closer to the pencil-thin approximation necessary to calculate the attenuation as shown in Section 2.2.2.

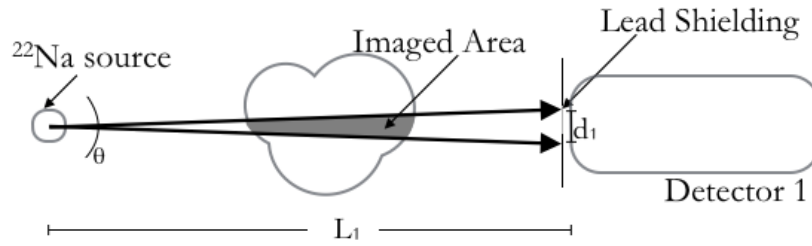


Figure 20. The addition of lead shielding with a hole of diameter d_1 decreases the angular width θ .

Since the count rate is directly proportional to the solid angle, it is important that the angular width of detectors 1 and 2 are the same. This allows for the maximum number of coincidences and smallest background for a given θ , and consequently allows for a shorter scanning time.

The holes drilled in the lead bricks measured $d_1=1.04$ cm and $d_2=0.81$ cm, so the ratio of L_2 to L_1 must be 40:51 to give the same angular acceptance for each detector. Thus if $L_1=30.5$ cm, L_2 must be 38.9 cm.

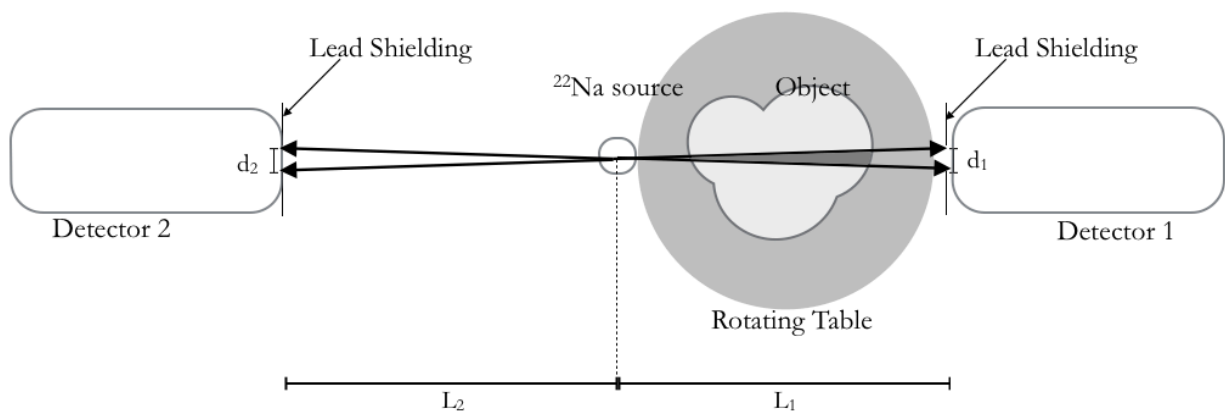


Figure 21. The distance the detectors are placed away from the ^{22}Na source depends on the diameter of the holes drilled in the lead shielding.

Chapter 4

CONCLUSION

4.1 Summary

The use of a low-activity ^{22}Na source in the construction of this CT scanner allows for less radiation exposure. However, because the source was low activity, background radiation would have been significant if a typical first generation CT scanner design was used. In order to reduce the effect of background radiation, two detectors were used in coincidence.

The ^{22}Na source produces positrons that annihilate to produce two antiparallel 0.511 MeV gamma rays. In order to allow the maximum number of coincidences, two NaI detectors were placed in line with the source and positioned so that the angular acceptance of each detector was the same.

LabVIEW software was used to count the number of gamma ray coincidences as well as for translating and rotating a robotic table positioned between the ^{22}Na source and one of the detectors. Ultimately, the same program can be used to determine the attenuation of the gamma rays by an object placed on the table and to reconstruct an image from the attenuation data collected.

4.2 Future Plans

Because it is likely that the project will be put on hold for a few years, the alignment of detectors and setup of electronics will need to be repeated.

The LabVIEW vi codes currently being used should be modified to continuously gather data. The vi must count the number of coincidences N seen during a specified time t along one beam path through the object, translate and rotate the table, and then collect the number of coincidences seen during the same time period t for each new beam path. The output of this data should be in the form of a matrix, where the attenuation measured along each beam that passes through an object is added to the sum for each voxel (as shown in Figure 10).

MatLab can then be used to convert this matrix into a gray scale image, where higher attenuation coefficients are represented by darker shades. When used together, the MatLab commands `colormap(gray)` and `imagesc(A)` can provide a scaled image of the matrix A where the lowest data values in the matrix are represented as black and the highest values are represented as white.

LabVIEW Block Diagram

The diagram illustrates a LabVIEW control system for a stepper motor. It features two DAQ Assistant blocks on the left, which interface with a Coincidence block and a Time Target block. The main logic on the right involves a Motor Number block, a Buffer Address block, and a Current Step block, all of which are connected to a large motor control block. This block has multiple inputs for steps, direction, and current step, and outputs for motor number, buffer address, and current step. The diagram is titled 'Stepper Motor Control' and includes a 'National Instruments' logo.

34

The second sequence in the structure moves the robotic table horizontally, and then rotates the table.

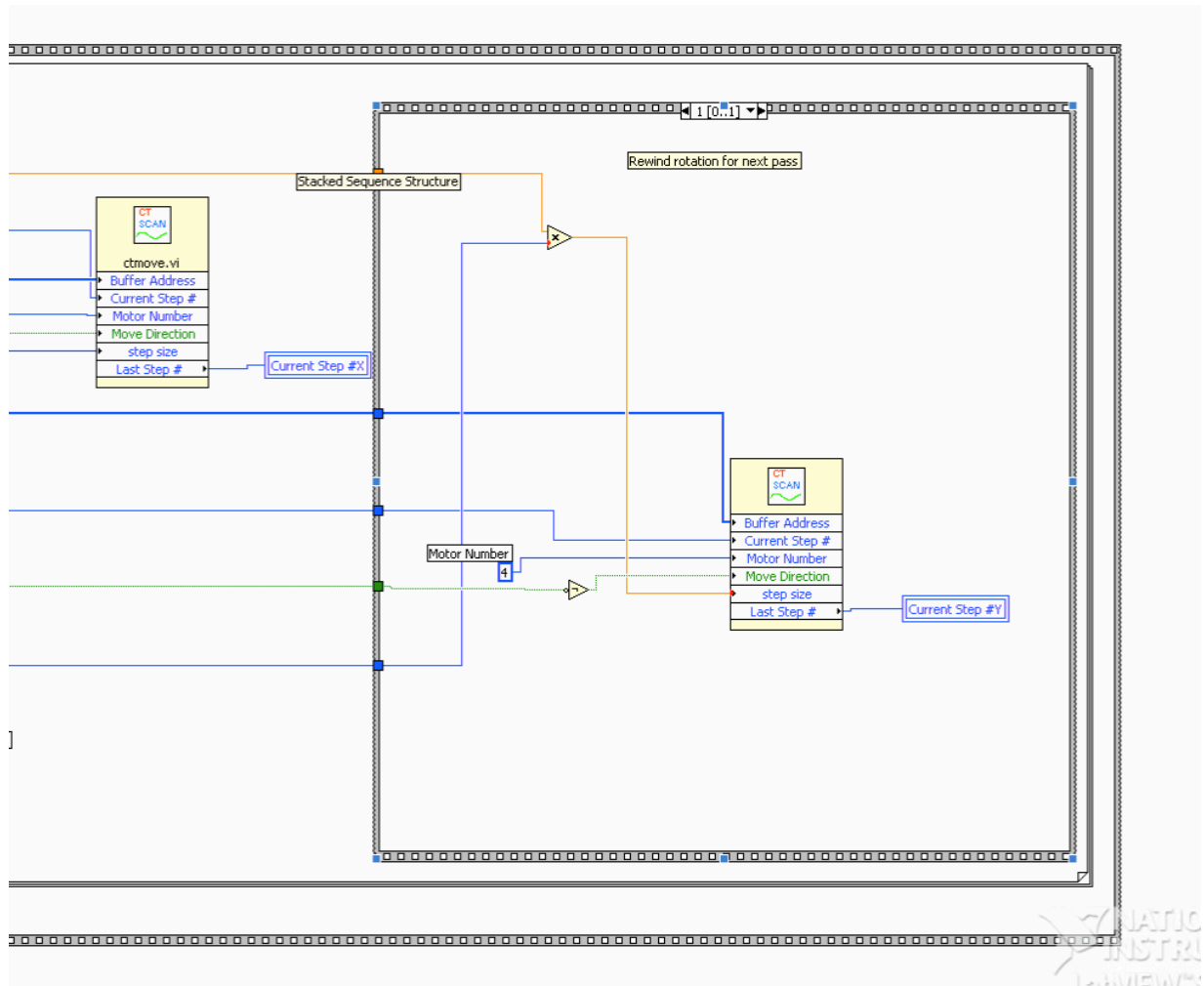


Figure 23. A partial screenshot of the LabVIEW block diagram used. Within the second frame of the sequence structure, a stacked sequence structure rotates and rewinds the table after it is moved horizontally.

References

- [1] J. T. Bushberg and J. M. Boone, *The Essential Physics of Medical Imaging*, 3rd Ed. (Lippincott Williams & Wilkins, Philadelphia, 2012).
- [2] W.C. Röntgen, Ann. Physik (Leipzig) **300**, 1 (1898).
- [3] W. R. Hendee and E. R. Ritenour, *Medical Imaging Physics*, 4th Ed. (Wiley, New York, 2002). p. 252.
- [4] G. N. Hounsfield, J. Comput. Assisted Tomography **4**, 5 (1980).
- [5] W. G. Bradley, Pro. Am. Philos. Soc. **152**, 3 (2008).
- [6] A. M. Cormack, Science **209**, 4464 (1980).
- [7] A. M. Cormack, Phys. Med. Biol. **18**, 2 (1973).
- [8] G. N. Hounsfield, J. Radiologie **61**, 6-7 (1980).
- [9] W. R. Hendee and E. R. Ritenour, *Medical Imaging Physics*, 4th Ed. (Wiley, New York, 2002). p. 256.
- [10] D. L. Bailey, P. J. Roach, E. A. Bailey, J. Hewlett, and R. Keijzers, Eur. J. Nucl. Med. Mol. Imaging **34**, 9 (2007).
- [11] D. R. Bernier, P. E. Christian, J. K Langan, and L. D. Wells, *Nuclear Medicine Technology and Techniques* (C. V. Mosby, Baltimore, 1989).
- [12] W. R. Hendee and E. R. Ritenour, *Medical Imaging Physics*, 4th Ed. (Wiley, New York, 2002). p. 255.
- [13] J. T. Bushberg and J. M. Boone, *The Essential Physics of Medical Imaging*, 3rd Ed. (Lippincott Williams & Wilkins, Philadelphia, 2012), p. 354.
- [14] J. T. Bushberg and J. M. Boone, *The Essential Physics of Medical Imaging*, 3rd Ed. (Lippincott Williams & Wilkins, Philadelphia, 2012), p. 352.